

A Non-Stationary MIMO Channel Model for Street Corner Scenarios Considering Velocity Variations of the Mobile Station and Scatterers

Ji Bian¹, Yu Liu¹, Cheng-Xiang Wang², Jian Sun¹, Wensheng Zhang¹, and Minggao Zhang¹

¹ Shandong Provincial Key Lab of Wireless Communication Technologies,

School of Information Science and Engineering, Shandong University, Jinan, 250100, China.

²Institute of Sensors, Signals and Systems, School of Engineering & Physical Sciences, Heriot-Watt University, Edinburgh, EH14 4AS, UK.
Email: {bianjimail, xinwenliuyu}@163.com, cheng-xiang.wang@hw.ac.uk, {sunjian, zhangwsh}@sdu.edu.cn, zmg225@163.com

Abstract—Most channel models in the literature assume that the scatterers are fixed and the mobile station (MS) moves with a constant speed in a given direction. However, in realistic propagation environments, both the scatterers and the MS can be moving, and the velocities of the scatterers and the MS can change with time. In this paper, we develop a non-stationary multiple-input multiple-output (MIMO) channel model for street corner scenarios. The proposed channel model takes into account both fixed and moving scatterers. Velocity variations, including speed and movement direction, of the MS and moving scatterers are considered. Analytical solutions of spatial cross-correlation function (CCF), temporal autocorrelation function (ACF), and Wigner-Ville spectrum are derived and analyzed. Moreover, the impacts of velocity variations on the statistical properties of the proposed model are investigated. The proposed channel model is illuminating for future vehicle-to-infrastructure (V2I) and vehicle-to-vehicle (V2V) channel modeling.

Index Terms—Non-stationary MIMO channel model, velocity variations, time-variant parameters, statistical properties, street corner scenarios.

I. INTRODUCTION

The V2V and V2I communications have drawn increasing attention from researchers in recent years and are considered to play a crucial role in the next-generation intelligent transportation systems (ITSs) [1], [2]. The V2V and V2I communications are assumed to provide many benefits, such as reducing traffic accidents and improving traffic efficiency. For example, in street corner scenarios, as illustrated in Fig. 1, drivers usually have poor visibility of the road. Real-time road condition information provided through extremely low latency V2I/V2V communications can help to avoid a collision. For system design and performance evaluation, detailed and accurate knowledge of the channels for street corner scenarios is necessary.

Most existing channel models are assumed to satisfy the wide-sense stationary (WSS) assumption, which means the stationarity of the channel during the observation time interval is fulfilled in the wide sense [3]. However, channels in realistic environments, especially in high mobility scenarios illustrate non-stationary properties [4]–[7]. Authors in [8] reported that the WSS assumption can result in erroneous evaluation of system performance. Therefore, for high mobility scenarios,

the non-stationarity of channels in channel modeling has to be considered. Most non-stationary channel models in the literature were developed based on the movements of the MS and clusters. Authors in [9] proposed a non-stationary IMT-Advanced high-speed train (HST) channel model [10]. Time-varying parameters including delays, powers, and angles were calculated according to the movement of the receiver and clusters. A three-dimensional (3-D) wideband non-stationary geometry-based stochastic channel model (GBSM) for V2V channels was proposed in [11]. The model is composed of a line-of-sight (LoS) component, a two-sphere model, and an elliptic-cylinder model. The last two models capture the effects of moving vehicles and fixed roadside scatterers, respectively. The movements of the transmitter and receiver result in time-varying angles of departure (AoDs) and time-varying angles of arrival (AoAs), which can be obtained based on the geometric construction.

A common assumption in the channel modeling is that the MS moves along a straight line with a constant speed. However, in real-world environments, the MS can move along different trajectories with time-varying speed. Relaxing the constant velocity assumption can help to develop more realistic non-stationary channel models. In [12], a non-stationary channel model for isotropic scattering environments considering velocity variations of the MS was proposed. The temporal ACF and Wigner-Ville spectrum of the proposed model were derived. In [13], a non-stationary mobile-to-mobile (M2M) channel model allowing for velocity variations of the MS was proposed. The authors developed the model under isotropic scattering condition and illustrated that the correlation properties of the M2M channel can be significantly affected by the variations of the MS velocity. Further extension of [13] were reported in [14], where the correlation properties of the proposed model were investigated under non-isotropic scattering condition. However, models in [13], [14] are single-input single-output (SISO) M2M channel models and the models in [12]–[14] omitted the moving scatterers in propagation environments.

In this paper, a non-stationary MIMO channel model for street corner scenarios is developed using a geometry-based

approach. The proposed model takes into account both fixed and moving scatterers, which correspond to the roadside buildings and moving vehicles, respectively. The movements of the MS and moving scatterers result in time-varying AoDs and AoAs, which make the model non-stationary. The contributions of this paper are summarized as follows.

(1) This paper proposes a non-stationary MIMO channel model for street corner scenarios. The velocity variations of the MS and scatterers are considered, which makes the model more general and realistic.

(2) From the proposed model, we derive the statistical properties including spatial CCF, temporal ACF, and Wigner-Ville spectrum, which are sufficiently general and can incorporate the effects of velocity variations of the MS and scatterers.

The remainder of this paper is organized as follows. Section II describes the geometric corner scattering channel model and gives the expression of the channel impulse response (CIR). Statistical properties of the model are studied in Section III. Section IV presents some numerical and simulation results. Finally, conclusions are drawn in Section V.

II. A NEW GBSM FOR STREET CORNER SCENARIOS

The narrowband MIMO geometric street corner scattering channel model is shown in Fig. 1. It is assumed that there are N_1 effective scatterers denoted by $S^{(n_1)}$ ($n_1 = 1, \dots, N_1$) lie on the buildings W_1 located on the right side of this figure, and N_2 effective scatterers denoted by $S^{(n_2)}$ ($n_2 = 1, \dots, N_2$) lie on the buildings W_2 located at the bottom of this figure. The moving vehicles or pedestrians in the propagation environment are modeled as N_3 effective scatterers which are denoted by $S^{(n_3)}$ ($n_3 = 1, \dots, N_3$). We assume that the base station (BS) is fixed. The MS and $S^{(n_3)}$ can be moving with time-varying velocities, including time-varying speeds and time-varying angles of motion (AoMs). The antenna array orientation of the MS is changed with the AoM of the MS. Both the BS and MS are equipped with uniform linear array with omnidirectional antennas. It is worth to mention that only the LoS component, and single-bounced (SB) components are considered in this model. The key parameters of this model are summarized in Table I.

The MIMO fading channel can be expressed as a matrix $\mathbf{H}(t) = [h_{pq}(t)]_{M_T \times M_R}$. The received complex fading envelope between the p -th ($p = 1, \dots, M_T$) transmit antenna element T_p and the q -th ($q = 1, \dots, M_R$) receive antenna element R_q is a superposition of the LoS component $h_{pq}^{\text{LoS}}(t)$ and non-line-of-sight (NLoS) component $h_{pq}^{\text{NLoS}}(t)$. The latter is composed of SB rays caused by fixed scatterers $h_{pq}^{\text{F}_i}(t)$, and SB rays caused by moving scatterers $h_{pq}^{\text{M}}(t)$. The CIR of the proposed model is given by

$$\begin{aligned} h_{pq}(t) &= h_{pq}^{\text{LoS}}(t) + h_{pq}^{\text{NLoS}}(t) \\ &= h_{pq}^{\text{LoS}}(t) + \sum_{i=1}^2 h_{pq}^{\text{F}_i}(t) + h_{pq}^{\text{M}}(t) \end{aligned} \quad (1)$$

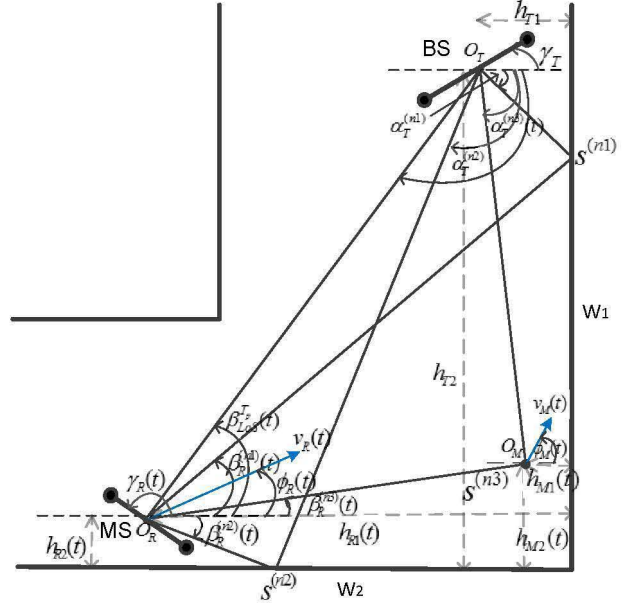


Fig. 1: The geometric corner scattering model containing fixed and moving scatterers.

where

$$\begin{aligned} h_{pq}^{\text{LoS}}(t) &= \sqrt{\frac{K_{pq} \cdot \Omega_{pq}}{K_{pq} + 1}} \cdot e^{-j k_0 \cdot \xi_{pq}(t)} \\ &\quad \cdot e^{j 2\pi \cdot \Phi_{\text{LoS}}(t)} \end{aligned} \quad (2)$$

$$\begin{aligned} h_{pq}^{\text{F}_i}(t) &= \sqrt{\frac{\eta_i \cdot \Omega_{pq}}{K_{pq} + 1}} \lim_{N_i \rightarrow \infty} \sum_{n_i=1}^{N_i} \frac{1}{\sqrt{N_i}} \\ &\quad e^{j(\theta_{n_i} - k_0 \cdot \xi_{pq,n_i}(t))} \cdot e^{j 2\pi \cdot \Phi_{\text{F}_i}(t)} \quad i = 1, 2 \end{aligned} \quad (3)$$

$$\begin{aligned} h_{pq}^{\text{M}}(t) &= \sqrt{\frac{\eta_3 \cdot \Omega_{pq}}{K_{pq} + 1}} \lim_{N_3 \rightarrow \infty} \sum_{n_3=1}^{N_3} \frac{1}{\sqrt{N_3}} \cdot e^{j(\theta_{n_3} - k_0 \cdot \xi_{pq,n_3}(t))} \\ &\quad \cdot e^{j 2\pi \cdot \Phi_{\text{M}_1}(t)} \cdot e^{-j 2\pi \cdot (\Phi_{\text{M}_2}(t) + \Phi_{\text{M}_3}(t))}. \end{aligned} \quad (4)$$

In (2)–(4), K_{pq} is the Ricean factor and Ω_{pq} is the total power of T_p-R_q link. Here, η_1 , η_2 , and η_3 designate how much the rays caused by fixed scatterers and moving scatterers contribute to the total scattered power $\Omega_{pq}/(K_{pq} + 1)$, respectively, and meet the condition $\eta_1 + \eta_2 + \eta_3 = 1$. $k_0 = 2\pi/\lambda$ is the wave number, where λ is wavelength. The initial phases θ_{n_1} , θ_{n_2} , and θ_{n_3} are independent and identically distributed (i.i.d.) random variables and uniform distributed from $-\pi$ to π . The time-varying Doppler frequency components caused by the moving MS and $S^{(n_3)}$ have to be expressed as integral forms

$$\Phi_{\text{LoS}}(t) = \int_0^t \frac{v_R(t)}{\lambda} \cdot \cos(\beta_{\text{LoS}}^{T_p}(t) - \phi_R(t)) dt \quad (5)$$

TABLE I: Summary of key parameter definitions.

δ_T, δ_R	antenna element spacings at the BS and MS, respectively
$\gamma_T, \gamma_R(t)$	antenna tilt angles at the BS and MS, respectively
$v_R(t), v_M(t)$	speeds of the MS and $S^{(n_3)}$, respectively
$\phi_R(t), \phi_M(t)$	AoMs of the MS and $S^{(n_3)}$, respectively
a_R, a_M	accelerations of the MS and $S^{(n_3)}$, respectively
ω_R, ω_M	angular speeds of the MS and $S^{(n_3)}$, respectively
$\alpha_T^{(n_i)}, \alpha_T^{(n_3)}(t) (i = 1, 2)$	AoDs of the waves impinging on $S^{(n_i)}$ and $S^{(n_3)}$, respectively
$\beta_R^{(n_i)}(t) (i = 1, 2, 3)$	AoAs of the waves traveling from $S^{(n_i)}$
$\beta_{\text{LoS}}^{T_p}(t)$	AoA of the LoS path
$\xi_{pq}(t), \xi_{pn_i}(t), \xi_{n_iq}(t), h_{T1(2)},$ and $h_{R(M)1(2)}(t) (i=1,2,3)$	distances $d(T_p, R_q)$, $d(T_p, S^{(n_i)})$, $d(S^{(n_i)}, R_q)$, $d(O_T, W_{1(2)})$, and $d(O_{R(M)}, W_{1(2)})$

$$\Phi_{F_i}(t) = \int_0^t \frac{v_R(t)}{\lambda} \cdot \cos(\beta_R^{(n_i)}(t) - \phi_R(t)) dt \quad (i = 1, 2) \quad (6)$$

$$\Phi_{M_1}(t) = \int_0^t \frac{v_R(t)}{\lambda} \cdot \cos(\beta_R^{(n_3)}(t) - \phi_R(t)) dt \quad (7)$$

$$\Phi_{M_2}(t) = \int_0^t \frac{v_M(t)}{\lambda} \cdot \cos(\alpha_T^{(n_3)}(t) - \phi_S(t)) dt \quad (8)$$

$$\Phi_{M_3}(t) = \int_0^t \frac{v_M(t)}{\lambda} \cdot \cos(\beta_R^{(n_3)}(t) - \phi_S(t)) dt. \quad (9)$$

The time-varying speed of the MS ($S^{(n_3)}$) can be calculated as

$$v_{R(M)}(t) = v_{R(M)}(t_0) + a_{R(M)} \cdot t \quad (10)$$

where t_0 indicates initial time. Similarly, the time-varying AoM of the MS ($S^{(n_3)}$) can be expressed as

$$\phi_{R(M)}(t) = \phi_{R(M)}(t_0) + \omega_{R(M)} \cdot t. \quad (11)$$

In (2)–(4), $\xi_{pq}(t)$ and $\xi_{pq,n_i}(t) = \xi_{pn_i}(t) + \xi_{n_iq}(t)$ are time-varying travel distances of the waves through the link $T_p - R_q$ and $T_p - s^{(n_i)} - R_q$, respectively. Note that $\min\{\xi_{TR}, \xi_{Tn_i}, \xi_{n_iR}\} \gg \max\{\delta_T, \delta_R\}$, the travel distances can be calculated as

$$\xi_{pq}(t) \approx \xi_{pR}(t) - k_q \delta_R \cos(\gamma_R(t) - \beta_{\text{LoS}}^{T_p}(t)) \quad (12)$$

$$\xi_{pn_{1(2)}} \approx \xi_{Tn_{1(2)}} - k_p \delta_T \cos(\gamma_T - \alpha_T^{(n_{1(2)})}) \quad (13)$$

$$\xi_{n_{1(2)}q}(t) \approx \xi_{n_{1(2)}R}(t) - k_q \delta_R \cos(\gamma_R(t) - \beta_R^{(n_{1(2)})}(t)) \quad (14)$$

$$\xi_{pn_3}(t) \approx \xi_{Tn_3}(t) - k_p \delta_T \cos(\gamma_T - \alpha_T^{(n_3)}(t)) \quad (15)$$

$$\xi_{n_3q}(t) \approx \xi_{n_3R}(t) - k_q \delta_R \cos(\gamma_R(t) - \beta_R^{(n_3)}(t)) \quad (16)$$

where $k_p = (M_T - 2p + 1)/2$ and $k_q = (M_R - 2q + 1)/2$,

$$\xi_{pR}(t) \approx \xi_{TR}(t) + k_p \delta_T \cos(\beta_{\text{LoS}}^{T_p}(t) - \gamma_T) \quad (17)$$

$$\xi_{TR}(t) = \sqrt{[h_{R1}(t) - h_{T1}(t)]^2 + [h_{R2}(t) - h_{T2}(t)]^2} \quad (18)$$

$$\xi_{Tn_1} = h_{T1}/\cos(\alpha_T^{(n_1)}) \quad (19)$$

$$\xi_{n_1R}(t) = h_{R1}(t)/\cos(\beta_R^{(n_1)}(t)) \quad (20)$$

$$\xi_{Tn_2} = h_{T2}/\sin(-\alpha_T^{(n_2)}) \quad (21)$$

$$\xi_{n_2R}(t) = h_{R2}(t)/\sin(-\beta_R^{(n_1)}(t)) \quad (22)$$

$$\xi_{Tn_3}(t) = \sqrt{[h_{M1}(t) - h_{T1}(t)]^2 + [h_{M2}(t) - h_{T2}(t)]^2} \quad (23)$$

$$\xi_{n_3R}(t) = \sqrt{[h_{M1}(t) - h_{R1}(t)]^2 + [h_{M2}(t) - h_{R2}(t)]^2}. \quad (24)$$

Based on the geometric construction, $\alpha_T^{(n_1)}$ is in the range of $(-\pi/2, 0)$, and $\alpha_T^{(n_2)}$ is in the range of $(-\pi, -\pi/2)$. For SB rays, the AoDs and the AoAs are interdependent. The AoAs can be calculated based on the AoDs and the movements of the MS and $S^{(n_3)}$. **For fixed clusters, the relationship between $\alpha_T^{(n_1)}$ and $\beta_R^{(n_1)}(t)$ and the relationship between $\alpha_T^{(n_2)}$ and $\beta_R^{(n_2)}(t)$ can be calculated as**

$$\beta_R^{(n_1)}(t) = \arctan\left(\frac{h_{T2} - h_{R2}(t) + \tan(\alpha_T^{(n_1)}) \cdot h_{T1}}{h_{R1}(t)}\right) \quad (25)$$

$$\beta_R^{(n_2)}(t) = \arccot\left(\frac{h_{T1} - h_{R1}(t) + \cot(\alpha_T^{(n_2)}) \cdot h_{T2}}{h_{R2}(t)}\right). \quad (26)$$

The moving cluster $S^{(n_3)}$ is depicted as a disc with a certain angular spread distributed in the horizontal plane. The relationship between $\alpha_T^{(n_3)}(t)$ and $\beta_R^{(n_3)}(t)$ can be determined as

$$\beta_R^{(n_3)}(t) = \arctan\left(\frac{\tan(\alpha_T^{(n_3)}(t) - \mu_T^{(2)}(t)) \cdot \xi_{Tn_3}(t)}{\xi_{n_3R}(t)}\right) + \mu_R^{(3)}(t) \quad (27)$$

where

$$\mu_T^{(3)}(t) = \arctan\left(\frac{h_{M1}(t) - h_{T1}(t)}{h_{T2}(t) - h_{M2}(t)}\right) \quad (28)$$

$$\mu_R^{(3)}(t) = \arctan\left(\frac{h_{M2}(t) - h_{R2}(t)}{h_{R1}(t) - h_{M1}(t)}\right). \quad (29)$$

III. STATISTICAL PROPERTIES

A. Spatial-Temporal Correlation Function

The spatial-temporal correlation function of CIR [15] can be defined as

$$\rho_h(t, \delta_T, \delta_R, \Delta t) = \frac{\mathbb{E}\{h_{p'q'}^*(t - \frac{\Delta t}{2}) h_{pq}(t + \frac{\Delta t}{2})\}}{\sqrt{\Omega_{p'q'} \Omega_{pq}}} \quad (30)$$

where $\mathbb{E}\{\cdot\}$ is expectation operator and $(\cdot)^*$ denotes the complex conjugate operation. Since the clusters in the proposed

models are assumed to be independent of each other, the spatial-temporal correlation function can be further expressed as the summation of the LoS component, fixed cluster component, and moving cluster component:

$$\rho_h(t, \delta_T, \delta_R, \Delta t) = \rho_h^{\text{LoS}}(t, \delta_T, \delta_R, \Delta t) + \sum_{i=1}^2 \rho_h^{F_i}(t, \delta_T, \delta_R, \Delta t) + \rho_h^M(t, \delta_T, \delta_R, \Delta t). \quad (31)$$

B. Spatial CCF

By substituting (1) to (31) and imposing $\Delta t = 0$, the spatial CCF can be obtained as

$$\rho_h(t, \delta_T, \delta_R) = \rho_h^{\text{LoS}}(t, \delta_T, \delta_R) + \sum_{i=1}^2 \rho_h^{F_i}(t, \delta_T, \delta_R) + \rho_h^M(t, \delta_T, \delta_R). \quad (32)$$

For the spatial CCF of the LoS component,

$$\rho_h^{\text{LoS}}(t, \delta_T, \delta_R) = \sqrt{\frac{K_{pq} K_{p'q'}}{(K_{pq} + 1)(K_{p'q'} + 1)}} \cdot e^{jk_0 \{ Q \cdot \cos(\beta_{\text{LoS}}^{T_p}(t) - \gamma_R(t)) - P \cdot \cos(\beta_{\text{LoS}}^{T_p}(t) - \gamma_T(t)) \}} \quad (33)$$

where $P = (p' - p)\delta_T/\lambda$, $Q = (q' - q)\delta_R/\lambda$. For the spatial CCF of the NLoS component,

$$\rho_h^{\text{NLoS}}(t, \delta_T, \delta_R) = \sum_{i=1}^2 \rho_h^{F_i}(t, \delta_T, \delta_R) + \rho_h^M(t, \delta_T, \delta_R) \quad (34)$$

and can be calculated as

$$\rho_h^{\text{NLoS}}(t, \delta_T, \delta_R) = \frac{\eta_i}{\sqrt{(K_{pq} + 1)(K_{p'q'} + 1)}} \int_{-\pi}^{\pi} e^{jk_0 \{ P \cdot \cos(\alpha_T^{(n_i)}(t) - \gamma_T) + Q \cdot \cos(\beta_R^{(n_i)}(t) - \gamma_R(t)) \}} \cdot p(\alpha_T^{(n_i)}) d\alpha_T^{(n_i)} \quad (i = 1, 2, 3) \quad (35)$$

where $p(\alpha_T^{(n_i)})$ is the probability density function (PDF) of $\alpha_T^{(n_i)}$.

C. Temporal ACF

The temporal ACF is calculated by substituting (1) to (31) and imposing $\delta_T = 0$ and $\delta_R = 0$, and can be expressed as

$$\rho_h(t, \Delta t) = \rho_h^{\text{LoS}}(t, \Delta t) + \sum_{i=1}^2 \rho_h^{F_i}(t, \Delta t) + \rho_h^M(t, \Delta t). \quad (36)$$

For the LoS component,

$$\rho_h^{\text{LoS}}(t, \Delta t) = \frac{K_{pq}}{K_{pq} + 1} e^{jk_0 (\xi_{qp}(t - \frac{\Delta t}{2}) - \xi_{qp}(t + \frac{\Delta t}{2}))} \cdot e^{j2\pi(\Phi_{\text{LoS}}(t + \frac{\Delta t}{2}) - \Phi_{\text{LoS}}(t - \frac{\Delta t}{2}))}. \quad (37)$$

For the SB component associated with fixed scatterers

$$\rho_h^{F_i}(t, \Delta t) = \frac{\eta_i}{K_{pq} + 1} \int_{-\pi}^{\pi} e^{jk_0 (\xi_{n_i R}(t - \frac{\Delta t}{2}) - \xi_{n_i R}(t + \frac{\Delta t}{2}))} \cdot e^{j2\pi(\Phi_{F_i}(t + \frac{\Delta t}{2}) - \Phi_{F_i}(t - \frac{\Delta t}{2}))} p(\alpha_T^{(n_i)}) d\alpha_T^{(n_i)} \quad (i = 1, 2). \quad (38)$$

For the SB component due to moving scatterers

$$\begin{aligned} \rho_h^M(t, \Delta t) = & \frac{\eta_3}{K_{pq} + 1} \int_{-\pi}^{\pi} e^{jk_0 (\xi_{pq, n_3}(t - \frac{\Delta t}{2}) - \xi_{pq, n_3}(t + \frac{\Delta t}{2}))} \\ & \cdot e^{j2\pi(\Phi_{M_1}(t + \frac{\Delta t}{2}) - \Phi_{M_1}(t - \frac{\Delta t}{2}))} \\ & \cdot e^{-j2\pi(\Phi_{M_2}(t + \frac{\Delta t}{2}) - \Phi_{M_2}(t - \frac{\Delta t}{2}))} \\ & \cdot e^{-j2\pi(\Phi_{M_3}(t + \frac{\Delta t}{2}) - \Phi_{M_3}(t - \frac{\Delta t}{2}))} \\ & \cdot p(\alpha_T^{(n_3)}, t) d\alpha_T^{(n_3)}. \end{aligned} \quad (39)$$

D. Wigner-Ville Spectrum

The Wigner-Ville spectrum [16] of the complex CIR is calculated through the Fourier transform of local temporal ACF in terms of Δt , and can be calculated as

$$\begin{aligned} S_h(t, f) = & \mathbb{E} \left\{ \int_{-\infty}^{\infty} h^*(t - \frac{\Delta t}{2}) h(t + \frac{\Delta t}{2}) \cdot e^{-j2\pi f \Delta t} d\Delta t \right\} \\ = & \int_{-\infty}^{\infty} \rho_h(t, \Delta t) \cdot e^{-j2\pi f \Delta t} d\Delta t. \end{aligned} \quad (40)$$

IV. RESULTS AND ANALYSIS

In this section, numerical and simulation results of statistics, i.e., spatial CCF, temporal ACF, and Wigner-Ville spectrum are presented. The AoDs and AoAs are assumed to follow von Mises distribution [17]. The PDF of von Mises distribution can be expressed as

$$f(x | \mu, \kappa) = \frac{e^{\kappa \cos(x - \mu)}}{2\pi I_0(\kappa)} \quad (41)$$

where $x \in [-\pi, \pi]$, $I_0(\cdot)$ denotes the zero order modified Bessel function of the first kind, μ is the mean value of angles, and κ controls the angular spread. The discrete values of angular parameters are obtained using the modified method of equal areas (MMEA) approach [18] and 50 cisoids are adopted in the simulation model. We assume that there are three clusters in the propagation environment. Two fixed clusters on the roadside buildings are located around transmitter and receiver, respectively, which contribute most to the received power. The third cluster is a moving cluster results from vehicles or pedestrians. The simulation parameters are selected as follows: $f = 2$ GHz, $M_T = 2$, $M_R = 2$, $\gamma_T = \pi/2$, $\gamma_R(t_0) = \pi/2$, $v_R(t_0) = 5$ m/s, $\phi_R(t_0) = 0$, $v_M(t_0) = 5$ m/s, $\phi_M(t_0) = 0$, $a_M = 0.2$ m/s², $\omega_M = \pi/20$ s⁻¹, $h_{T1} = 8$ m, $h_{T2} = 70$ m, $h_{R1}(t_0) = 60$ m, $h_{R2}(t_0) = 4$ m, $h_{S1}(t_0) = 80$ m, $h_{S2}(t_0) = 40$ m, $\mu^{(n_1)} = -\pi/4$, $\mu^{(n_2)} = -5\pi/9$, $\kappa^{(n_i)} = 10$ ($i = 1, 2, 3$), $K_{p,q} = 0$, $K_{p',q'} = 0$, $\eta_1 = 0.4$, $\eta_2 = 0.5$, $\eta_3 = 0.1$.

The absolute values of the time-varying spatial CCF are shown in Fig. 2. The spatial CCF varying with time t and caused by the velocity variations of the MS and the moving scatterers can be observed. The results in Fig. 3 are obtained when the MS travels along a straight line with an angular speed. The differences between the two curves stem from the time-varying antenna orientation of the MS. Besides, (33) and

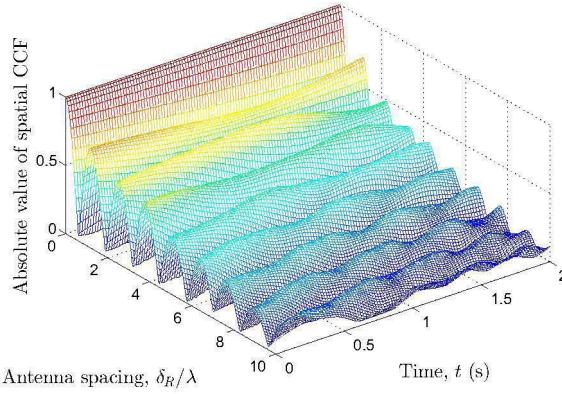


Fig. 2: The absolute value of the local spatial CCF of the proposed model ($v_R(t_0) = 5 \text{ m/s}$, $\phi_R(t_0) = 0$, $a_R = 0.2 \text{ m/s}^2$, $\omega_R = \pi/10 \text{ s}^{-1}$, $v_M(t_0) = 5 \text{ m/s}$, $\phi_M(t_0) = 0$, $a_M = 0.2 \text{ m/s}^2$, $\omega_M = \pi/20 \text{ s}^{-1}$).

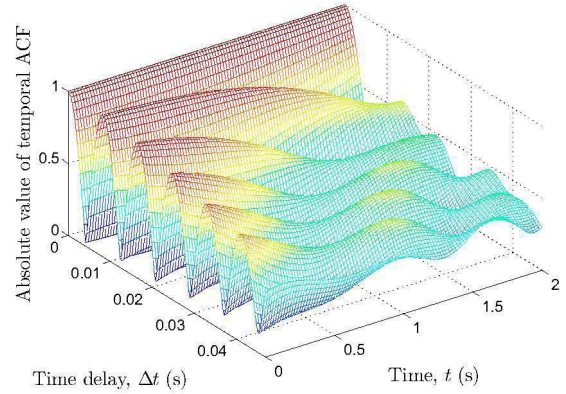


Fig. 4: The absolute value of the local temporal ACF of the proposed model ($v_R(t_0) = 5 \text{ m/s}$, $\phi_R(t_0) = 0$, $a_R = 0.2 \text{ m/s}^2$, $\omega_R = \pi/10 \text{ s}^{-1}$, $v_M(t_0) = 5 \text{ m/s}$, $\phi_M(t_0) = 0$, $a_M = 0.2 \text{ m/s}^2$, $\omega_M = \pi/20 \text{ s}^{-1}$).

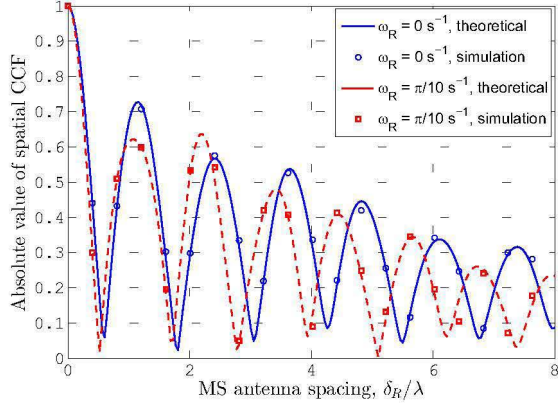


Fig. 3: The absolute value of the local spatial CCF of the proposed model at different angular speeds ($v_R(t_0) = 5 \text{ m/s}$, $\phi_R(t_0) = 0$, $a_R = 0.2 \text{ m/s}^2$, $v_M(t_0) = 5 \text{ m/s}$, $\phi_M(t_0) = 0$, $a_M = 0.2 \text{ m/s}^2$, $\omega_M = \pi/20 \text{ s}^{-1}$).

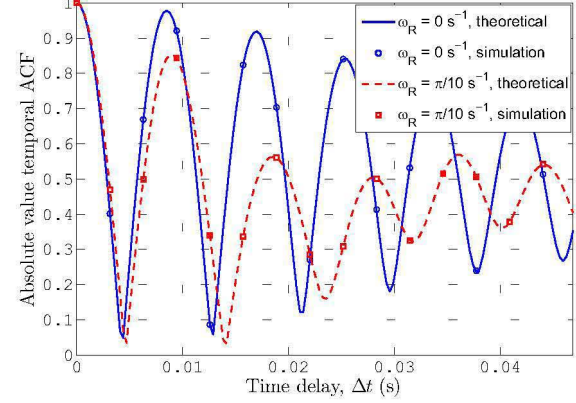


Fig. 5: The absolute value of the local temporal ACF of the proposed model at different angular speeds ($v_R(t_0) = 5 \text{ m/s}$, $\phi_R(t_0) = 0$, $a_R = 0.2 \text{ m/s}^2$, $v_M(t_0) = 5 \text{ m/s}$, $\phi_M(t_0) = 0$, $a_M = 0.2 \text{ m/s}^2$, $\omega_M = \pi/20 \text{ s}^{-1}$).

(35) indicate the acceleration have no influence on the spatial CCF.

Fig. 4 shows the absolute value of the time-varying temporal ACF of the proposed model. Both the movements of clusters and velocity variations (including acceleration and angular speed) result in time-varying ACF. Results of Fig. 5 and Fig. 6 show the influences of angular speed and acceleration of the MS on the temporal ACFs. We can find that both the angular speed and acceleration result in weak temporal correlation. Moreover, we find that the angular speed has a greater impact on the temporal correlation than that of the acceleration.

The Wigner-Ville spectrums of the proposed model at different angular speeds and accelerations are shown in Fig. 7. Compared with Fig. 7 (a), which is obtained when the MS moves along a straight line with a constant speed, Wigner-Ville spectrum varying over time due to the velocity variations

of the MS can be observed. The time-varying Wigner-Ville spectrum in Fig. 7 (b) is caused by the angular speed of the MS. In Fig. 7 (c), the speed of the MS increases when the MS moves with an acceleration, which results in increased values of Doppler frequency shifts. Fig. 7 (d) shows the combined effects of angular speed and acceleration of the MS on the Wigner-Ville spectrum of the proposed model.

V. CONCLUSIONS

In this paper, we have proposed a non-stationary MIMO channel model for street corner scenarios. The model was taken into account both fixed and moving scatterers. The speeds and trajectories of the MS and moving scatterers are allowed to change. All of these make the proposed model more general and flexible. Statistical properties including spatial CCF, temporal ACF, and Wigner-Ville spectrum have been

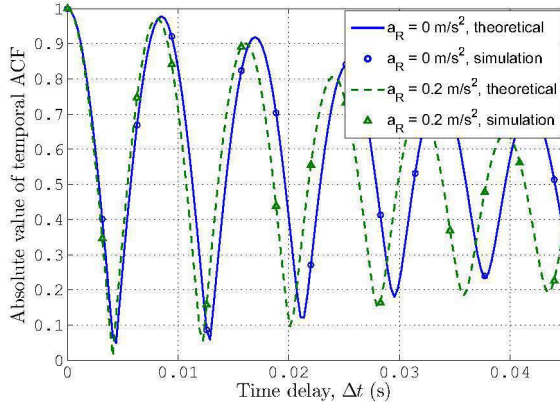


Fig. 6: The absolute value of the local temporal ACF of the proposed model at different accelerations ($v_R(t_0) = 5 \text{ m/s}$, $\phi_R(t_0) = 0$, $\omega_R = \pi/10 \text{ s}^{-1}$, $v_M(t_0) = 5 \text{ m/s}$, $\phi_M(t_0) = 0$, $a_M = 0.2 \text{ m/s}^2$, $\omega_M = \pi/20 \text{ s}^{-1}$).

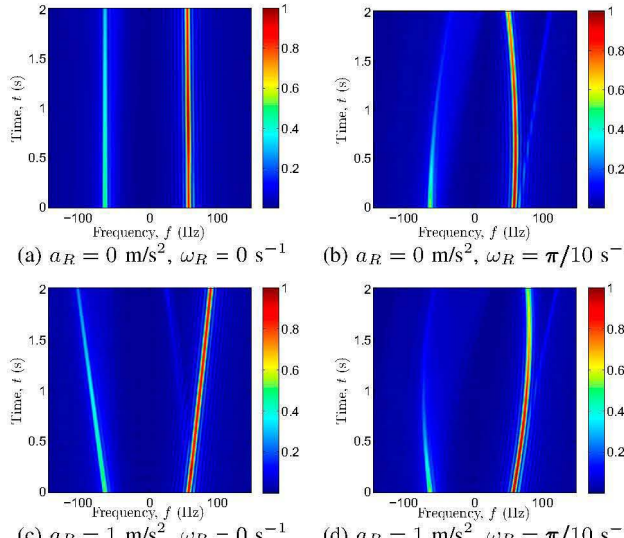


Fig. 7: Wigner-Ville spectrum of the proposed model at different angular speeds and accelerations ($v_R(t_0) = 5 \text{ m/s}$, $\phi_R(t_0) = 0$, $v_M(t_0) = 5 \text{ m/s}$, $\phi_M(t_0) = 0$, $a_M = 0.2 \text{ m/s}^2$, $\omega_M = \pi/20 \text{ s}^{-1}$).

derived. Numerical and simulation results have been presented and analyzed under the non-isotropic scattering condition. We have found that the velocity variations of the MS and moving scatterers can have significant influences on channel statistics and exacerbate the non-stationarity of the channels. The proposed model provides a fundamental framework for future non-stationary channel modeling.

ACKNOWLEDGEMENT

The authors gratefully acknowledge the support from the Natural Science Foundation of China (Grant No. 61371110), Fundamental Research Funds of Shandong University (2017JC009), EPSRC TOUCAN project (Grant No. EP/L020009/1), and EU H2020 RISE TESTBED project (Grant No. 734325).

REFERENCES

- [1] S. T. Cheng, G. J. Horng, and C. L. Chou, "Using cellular automata to form car society in vehicular ad hoc networks," *IEEE Trans. Intell. Transp. Syst.*, vol. 12, no. 4, pp. 1374–1384, Dec. 2011.
- [2] C.-X. Wang, X. Hong, X. Ge, X. Cheng, G. Zhang, and J. Thompson, "Cooperative MIMO channel models: A survey," *IEEE Commun. Mag.*, vol. 48, no. 2, pp. 80–87, Feb. 2010.
- [3] A. F. Molisch, *Wireless communications*. 2nd Edition, Chichester: John Wiley & Sons, 2012.
- [4] R. He, O. Renaudin, V. M. Kolmonen, K. Haneda, Z. Zhong, B. Ai, S. Hubert, and C. Oestges, "Vehicle-to-vehicle radio channel characterization in crossroad scenarios," *IEEE Trans. Veh. Technol.*, vol. 65, no. 8, pp. 5850–5861, Aug. 2016.
- [5] O. Renaudin, V. M. Kolmonen, P. Vainikainen, and C. Oestges, "Car-to-car channel models based on wideband MIMO measurements at 5.3 GHz," in *Proc. EuCAP'09*, Berlin, German, Mar. 2009, pp. 635–639.
- [6] Y. Liu, C.-X. Wang, C. F. Lopez, and X. Ge, "3D non-stationary wideband circular tunnel channel models for high-speed train wireless communication systems," *Sci. China Inf. Sci.*, vol. 60, no. 8, Aug. 2017, in press.
- [7] Y. Liu, A. Ghazal, C.-X. Wang, X. Ge, Y. Yang, and Y. Zhang, "Channel measurements and models for high-speed train wireless communication systems in tunnel scenarios: A survey," *Sci. China Inf. Sci.*, vol. 60, no. 8, Oct. 2017, in press.
- [8] D. W. Matolak, "Channel modeling for vehicle-to-vehicle communications," *IEEE Commun. Mag.*, vol. 46, no. 5, pp. 76–83, May 2008.
- [9] A. Ghazal, Y. Yuan, C. X. Wang, Y. Zhang, Q. Yao, H. Zhou, and W. Duan, "A non-stationary IMT-Advanced MIMO channel model for high-mobility wireless communication systems," *IEEE Trans. Wireless Commun.*, vol. 16, no. 4, pp. 2057–2068, Apr. 2017.
- [10] ITU-R M.2135-1, "Guidelines for evaluation of radio interface technologies for IMT-Advanced," Gneva, Switzerland, Rep. ITU-R M.2135-1, Dec. 2009.
- [11] Y. Yuan, C. X. Wang, Y. He, M. M. Alwakeel, and e. H. M. Aggoune, "3D wideband non-stationary geometry-based stochastic models for non-isotropic MIMO vehicle-to-vehicle channels," *IEEE Trans. Wireless Commun.*, vol. 14, no. 12, pp. 6883–6895, Dec. 2015.
- [12] M. Pätzold and A. Borhani, "A non-stationary multipath fading channel model incorporating the effect of velocity variations of the mobile station," in *Proc. WCNC'14*, Istanbul, Turkey, Apr. 2014, pp. 182–187.
- [13] W. Dahech, M. Pätzold, and N. Youssef, "A non-stationary mobile-to-mobile multipath fading channel model taking account of velocity variations of the mobile stations," in *Proc. EuCAP'15*, Lisbon, Portugal, May 2015, pp. 1–4.
- [14] W. Dahech, M. Pätzold, C. A. Gutierrez, and N. Youssef, "A non-stationary mobile-to-mobile channel model allowing for velocity and trajectory variations of the mobile stations," *IEEE Trans. Wireless Commun.*, vol. 16, no. 3, pp. 1987–2000, Mar. 2017.
- [15] C.-X. Wang, X. Hong, H. Wu, and W. Xu, "Spatial-temporal correlation properties of the 3GPP spatial channel model and the kronecker MIMO channel model," *EURASIP J. Wireless Commun. Netw.*, vol. 2007, no. 1, pp. 59–59, Jan. 2007.
- [16] L. Cohen, "Time-frequency distributions-a review," *Proc. IEEE*, vol. 77, no. 7, pp. 941–981, Jul. 1989.
- [17] A. Abdi and M. Kaveh, "A space-time correlation model for multielement antenna systems in mobile fading channels," *IEEE J. Sel. Areas Commun.*, vol. 20, no. 3, pp. 550–560, Apr. 2002.
- [18] C. A. G.-D. de Leon and M. Pätzold, "Sum-of-sinusoids-based simulation of flat fading wireless propagation channels under non-isotropic scattering conditions," in *Proc. IEEE GLOBECOM'07*, Washington DC, USA, Nov. 2007, pp. 3842–3846.